ACS OMEGA

http://pubs.acs.org/journal/acsodf

Article

Dynamic Evolution of Gas Flow during Coalbed Methane Recovery to Reduce Greenhouse Gas Emission: A Case Study

Haoran Song, Baiquan Lin, Zheng Zhong,* and Ting Liu

Cite This: *ACS Omega* 2022, 7, 29211−29222

Read Online

ACCESS | Metrics & More | Article Recommendations

ABSTRACT: Gas pre-extraction technology in a coal reservoir can not only reduce greenhouse gas (GHG) emissions but also effectively recover coalbed methane (CBM). In this work, we use a geomechanical-coupled gas flow (GCF) model to simulate and analyze the pre-extraction effect of a mining-disturbed coal seam. First, the simulation results of the GCF model are compared with field test data to verify the correctness and reliability of our model. Then, the evolution law of the stress field, permeability field, and gas flow field in the extraction process is analyzed through a case study. The results show that the first principal stress of coal in a mining area increases first and then decreases slowly and reaches the peak value at 5 m. The third principal stress increases gradually at first and becomes stable after 10 m. As the distance from the mining face increases, the permeability and gas pressure of the coal seam show continuous and asymmetric "U"-shaped and "n"-shaped distribution characteristics, respectively. In addition, the recovery effect and abnormal emission factors of CBM are discussed. This study can provide theoretical guidance for optimizing the CBM recovery effect and reducing GHG emissions during mining.

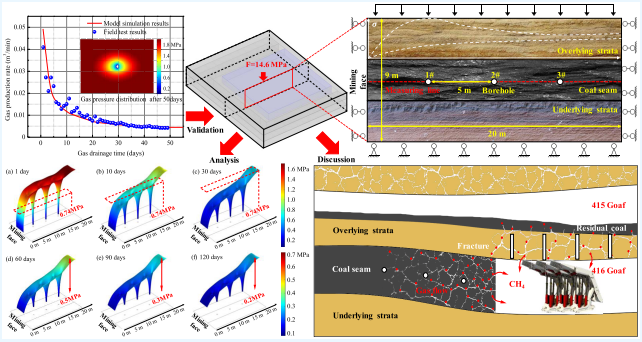

1. INTRODUCTION

Coalbed methane (CBM) is an associated gas produced during coal mining,[1] which is a kind of gas energy associated with coal,[2,3] but it is also a greenhouse gas (GHG) that causes environmental pollution.[4,5] In particular, large quantities of GHG are emitted during coal mining due to geomechanical instability. This will not only lead to the aggravation of the greenhouse effect but also lead to coal mine fires or gas explosions[6,7] and other dangerous accidents.[8,9] Therefore, how to effectively recover CBM resources and reduce GHG emissions is the focus and hotspot of current research.[10−12]

Gas pre-extraction technology and its derivative technology are widely used because of its engineering effectiveness.[13,14] Relevant studies show that it can effectively control greenhouse gas emissions and recover CBM in coal mining engineering.[4,15,16] In addition, the permeability of coal and the gas flow are the key factors affecting the recovery effect of the extraction borehole.[17,18] Because underground gas extraction engineering usually lasts for a long time, and the physical fields of coal seams, such as geological stress, permeability, gas flow, and temperature, affect each other and change continuously,[19,20] hence, the discovery of the dynamic evolution law of permeability and gas flow is critical for CBM recovery and GHG emission reduction.

To reveal the interaction between various physical fields during gas extraction, researchers have developed many multifield coupled permeability models. Zhang et al.[21] developed a new finite element permeability model, considering the influence of coal matrix deformation on permeability evolution, and the results show that adsorption volume expansion and effective stress are the main factors controlling permeability change. Based on the elastic medium theory, Lu et al.[22] established a dual-porosity model, verified the model through field test data, and applied the model to the permeability prediction of coal seams under different boundary conditions. Wang et al.[23] considered the Klinkenberg effect of gas flow in low-permeability reservoirs and improved the traditional coal bundled matchstick model, which can accurately predict CBM production. Peng et al.[24] defined the coefficient of expansion within the coal matrix, which corrected the change of permeability caused by volume expansion, and verified the improved model through experiments. Zhang et al.[25] established a fluid-solid coupling model considering the anisotropy of coal permeability, and then studied the influence of coal mechanical behavior on gas seepage field evolution through a combination of experimental and numerical

Received: May 26, 2022
Accepted: August 4, 2022
Published: August 11, 2022

https://doi.org/10.1021/acsomega.2c03274
ACS Omega 2022, 7, 29211−29222

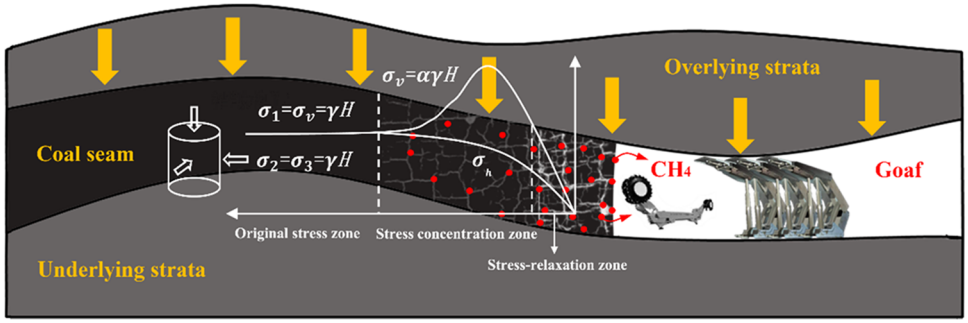

Figure 1. Illustration of gas flow in the mining-disturbed coal seam.

simulations. Dejam[26] developed a reduced-order model of convection−dispersion mass transfer in porous-walled microfluidic channels and studied the effects of different parameters on the mass transfer velocity of a fluid in the model channels. Fang et al.[27] analyzed the interaction between the coal matrix contraction and effective stress and established a mathematical model based on them, revealing the evolution law of coal seam permeability during the CO_2-ECBM process.

The large-scale emission of GHG mostly occurs near the coal face because the mining disturbance causes the continuous change of the coal stress state, which leads to the damage of the original coal and further affects the coal seam gas flow (see Figure 1). Xie et al.[28] studied the stress distribution characteristics under different mining methods, clarified the dynamic evolution process of the stress in a mining coal seam, and revealed the three-dimensional stress distribution rule of coal in the mining face. Xue et al.[29] carried out the mechanical property experiment of coal stress -damage, defined the damage factor according to the crack propagation degree of coal, and revealed the inducement of the gas outburst caused by mining disturbance. Based on the evolution law of coal permeability in the process of stress loading, Lu et al.[30] established the evolution model of damage-induced permeability. After analyzing the data of field gas extraction and simulation data, the reasonable layout of the underground gas extraction borehole is optimized. Zheng et al.[31] focused on the permeability change caused by coal damage, established a multifield coupling permeability model, and analyzed the influence of coal damage on the gas flow. To analyze the relationship between coal seam mining and gas desorption, An et al.[32] simulated the gas migration during coal seam excavation, and the results showed that stress release and fracture development occurred in coal near the mining face. Liu et al.[33] proposed an equivalent fractured coal model, quantified the cracks generated after coal damage, and established a permeability model suitable for the plastic deformation of damaged coal seams. Chen et al.[34] studied the ground stress and CBM pressure, two important parameters that affect gas disasters. The results show that these two parameters have significant zonal variation characteristics, which is of great significance for mining safety and environmental benefits.

Scholars have done a lot of meaningful work in coal permeability analysis and modeling, including experimental testing and numerical simulation analysis. However, there are a few studies on methane gas leakage in the coal mining face that consider coal damage and anisotropy, and the effectiveness of disturbed coal seam gas extraction needs further study. Figure 1 shows an illustration of gas flow in the mining-disturbed coal seam. As shown in the figure, due to mining disturbance, the stress state of coal changes constantly, leading to the destruction of coal next to the mining face. The damage to the coal results in a large amount of gas changing from a stable adsorption state to a free state, which leads to the dynamic evolution of gas seepage in the coal seam. To study the above problems, a multifield coupling model of the mechanical field and the gas flow field is established by considering the anisotropy of coal. Then, the evolution laws of the coal seam stress field, permeability field, and gas flow field are studied. Finally, by analyzing the variation characteristics of gas content in the coal seam and overlying strata, the design of gas extraction engineering in the mining-disturbed coal seam and goaf is discussed through a case study. This study can not only guide the layout of gas extraction boreholes but also provide engineering references for GHG emission reduction and CBM recovery.

2. MODELS AND THEORIES

2.1. Model Hypotheses. To make the established multifield coupling model conform to physical laws as much as possible and reduce the model calculation time, in this paper, the model meets the following hypotheses.[21,35,36]

(1) Coal is a dual-porosity medium with permeability anisotropy, which is composed of a coal skeleton, pores, and fractures.

(2) CBM is an ideal gas whose flow in fractures obeys Darcy's law, and the migration in the matrix follows Fick's law.

(3) Deformation of the coal is mainly linear elastic and the strain of the coal skeleton is infinitesimal.

(4) The temperature of the whole process is constant, and the effect of water content on coal permeability can be ignored.

2.2. Coal Deformation. Coal is a dual-porosity porous medium material and considers the influences of gas adsorption or desorption on coal deformation.[37] To better describe the mechanical deformation, the following modified constitutive equation is given

$$\sigma_{ij} = 2G\varepsilon_{ij} + \frac{2\mu G}{1-2\mu}\varepsilon_v - \alpha_f P_f - \alpha_p P_p - \sigma_a \quad (1)$$

where σ_{ij} represents the stress acting (MPa); G is the shear modulus, $G = \frac{E}{2(1+\mu)}$; ε_v denotes volumetric strain, $\varepsilon_v = \varepsilon_x + \varepsilon_y + \varepsilon_z$; P_f and P_p represent the gas pressures in fractures and pores; and α_f and α_p are effective stress coefficients of fractures and pores, as shown in 2. σ_a is swelling stress (MPa),

https://doi.org/10.1021/acsomega.2c03274
ACS Omega 2022, 7, 29211−29222

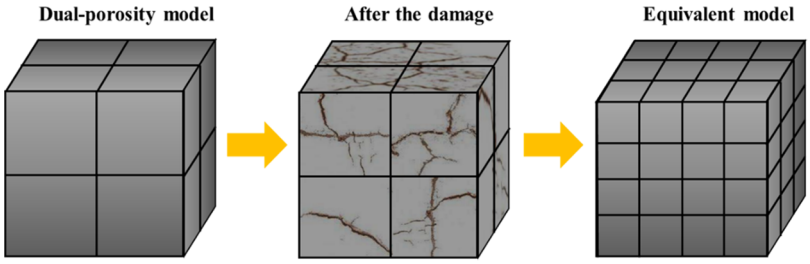

Figure 2. Illustration of the coal matrix before and after damage.

$\sigma_a = \frac{a\rho RT \ln(1 + bP_p)}{V_m}$,[38] where a and b are the maximum adsorption capacity (cm^3/g) and the Langmuir adsorption constant (MPa^{-1}); ρ is the density (Kg/cm^3); V_m is molar volume of gas; R is the molar gas constant; and T is the temperature (K).

$$\begin{cases} \alpha_f = 1 - \dfrac{E}{E_p} \\ \alpha_p = \dfrac{3\varphi_p(1-\mu)E}{2(1-2\mu)E_p} \end{cases} \tag{2}$$

where, μ and φ_p represent the Poisson's ratio and porosity (%), respectively, and E_p and E represent Young's modulus of the skeleton and coal (MPa), respectively.

According to the continuity assumption, the equilibrium equation and the geometric equation for the REV can be expressed as

$$\begin{cases} \sigma_{ij,i} + F_j = 0 \\ \varepsilon_{ij} = \dfrac{1}{2}(u_{i,j} + u_{j,i}) \end{cases} \tag{3}$$

where F_j represents the body force (MPa) and u_i is the displacement of coal.

By combining 1−3, we can get the gas-bearing coal deformation equation as follows

$$Gu_{i,ji} + \frac{2\mu G}{1-2\mu}\varepsilon_v - \alpha_f P_f - \alpha_p P_p - \sigma_a + F_j = 0 \tag{4}$$

2.3. Coal Damage Evolution. As the shearer advances forward, the stress state of coal in front of the mining face changes and the coal matrix is damaged. Figure 2 shows the illustration of the coal matrix before and after damage. From Figure 2, when the coal is damaged, the representative elementary volume of coal is broken and produces tiny fractures. Assuming that these fractures are uniformly distributed in the coal matrix, it can be considered that the original larger matrix unit is damaged and turns into many small-size matrix units.

Salari et al.[39] proposed that the plastic deformation damage of rocks was caused by volumetric strain expansion, and many scholars used an exponential function to represent the damage law of coal.[33,40] The damage equation is shown below

$$D = 1 - e^{-(\varepsilon^V - \varepsilon_1^V/F)^m} \tag{5}$$

where D is the coal damage factor; ε^V is the volume-dependent variable; ε_1^V is the volume strain threshold; m is the parameter of coal strength distribution, 2; and F is the coal strength parameter.

Based on the elastic damage theory, coal damage leads to effective stress changes. Then, the constitutive relation of coal damage is given as

$$\sigma_{ij} = E_{ij}(\varepsilon_{ij} - \varepsilon_{ij}^p)(1 - D) \tag{6}$$

where E_{ij} is the elastic modulus and ε_{ij}^p is the plastic strain variable.

2.4. Porosity and Permeability. Considering the uniaxial strain of porous media, Palmer[41] established a classical porosity evolution equation as

$$-d\varphi_f = \left[\frac{1}{M} - (1-\varphi_f)\beta\gamma\right](d\sigma - dp) + \left[\frac{K}{M} - (1-\varphi_f)\right]\gamma dp - \left[\frac{K}{M} - (1-\varphi_f)\right]\xi_t\, dT \tag{7}$$

where $M = \frac{(1-\mu)E}{(1+\mu)(1-2\mu)}$ and $K = \frac{E}{3(1-2\mu)}$ indicate axial and bulk moduli (MPa), φ_f is the porosity of fractures (%), β is the scale factor, γ is the compression coefficient (Pa^{-1}), p is the gas pressure (Pa), and ξ_t is the thermal expansion coefficient (F^{-1}).

We assume that the whole process is isothermal and the coal skeleton is incompressible, so dT and γ are 0. Therefore, 7 simplifies to

$$d\varphi_f = \frac{1}{M}(\alpha_f dP_f + \alpha_p dP_p + d\sigma_a) \tag{8}$$

By solving the differential 8, we have

$$\varphi_f = \varphi_{f0} + \frac{\alpha_f}{M}(P_f - P_{f0}) + \frac{\alpha_p}{M}(P_p - P_{p0}) + \frac{a\rho RT}{MV_m}\ln\left(\frac{1 + bP_{p0}}{1 + bP_p}\right) \tag{9}$$

Damage factors affect the permeability of coal,[42] and we establish the following relationship

$$\frac{k}{k_0} = (1 + D\xi)\left(\frac{\varphi_f}{\varphi_{f0}}\right)^3 \tag{10}$$

Since the airflow in the low-permeability coal seam obeys the Klinkenberg effect,[37] so we have

$$k = k_0\left(1 + \frac{c}{p_f}\right) \tag{11}$$

By combining 9−11, the coal permeability evolution model can be expressed as

https://doi.org/10.1021/acsomega.2c03274
ACS Omega 2022, 7, 29211−29222

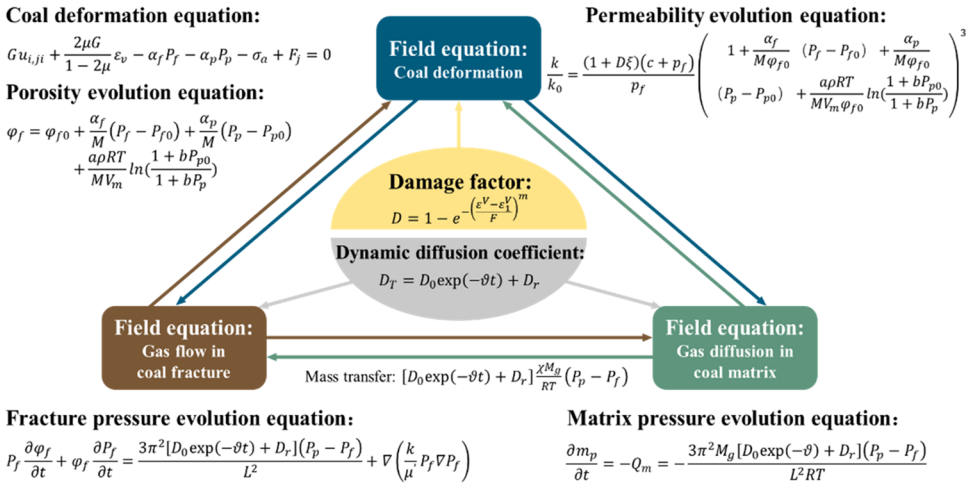

Figure 3. Cross-coupling model.

$$\frac{k}{k_0}=\frac{(1+D\xi)(c+p_f)}{p_f}\left(1+\frac{\alpha_f(P_f-P_{f0})}{M\varphi_{f0}}+\frac{\alpha_p(P_p-P_{p0})}{M\varphi_{f0}}+\frac{a\rho RT}{MV_m\varphi_{f0}}\ln\left(\frac{1+bP_{p0}}{1+bP_p}\right)\right)^3 \tag{12}$$

where k_0 represents the initial permeability of coal; ξ represents the skip coefficient; and c represents the Klinkenberg coefficient, $c = 0.95\ k_0 - 0.33$.

2.5. Gas Diffusion. The gas migration process of the coal seam consists of two stages: First, the gas in the matrix is desorbed gradually and diffuses into the fractures of coal. Second, due to the effect of the gas pressure difference, gas from the fractures seeps into the borehole. According to our previous research,[43] the diffusion coefficient is not a fixed value in the traditional model but a variable that decreases with the diffusion time

$$D_T = D_0\exp(-\vartheta t) + D_r \tag{13}$$

where ϑ is the attenuation coefficient, D_T and D_0 indicate the diffusion coefficient at time T and time 0, and D_r is the residual diffusion coefficient (m^2/s).

According to previous research,[42] the gas mass transport satisfies the following formula

$$Q_m = D_T\chi\frac{M_g}{RT}(P_p - P_f) \tag{14}$$

where χ indicates the shape factor, $\chi = \frac{3\pi^2}{L^2}$, and L is the fracture length. Moreover, M_g and Q_m denote the molar mass of methane and the gas exchange rate between pores and fractures ($kg/(m^3{\cdot}s)$), respectively.

The gas content per unit volume of the matrix is given as

$$m_p = \varphi_p\frac{M_g}{RT}P_p + \frac{\rho_c abP_pM_g}{(1+bP_p)V_m} \tag{15}$$

where m_p represents the gas mass per unit volume of the matrix (kg/m^3), φ_p represents the matrix porosity, and ρ_c indicates the apparent density of the coal.

By combining 13−15 and the conservation of mass, the governing equation of gas diffusion can be obtained as follows

$$\frac{\partial m_p}{\partial t} = -Q_m = -\frac{3\pi^2M_g[D_0\exp(-\vartheta t) + D_r](P_p - P_f)}{L^2RT} \tag{16}$$

2.6. Gas Flow. Assuming that the gas seepage is laminar, the velocity of gas flow can be stated by Darcy's law

$$v_f = -\frac{k}{\mu'}\nabla P_f \tag{17}$$

where μ' represents the gas dynamic viscosity (Pa·s).

Based on the law of conservation of mass, we have

$$\frac{\partial\varphi_f P_f}{\partial t} = Q_m(1-\varphi_f) - \nabla\left(\frac{M_gP_f}{RT}v_f\right) \tag{18}$$

By substituting 14 and 17 into 18, the simplified gas flow governing equation is given as follows

$$P_f\frac{\partial\varphi_f}{\partial t} + \varphi_f\frac{\partial P_f}{\partial t} = \frac{3\pi^2[D_0\exp(-\vartheta t) + D_r](P_p - P_f)}{L^2} + \nabla\left(\frac{kP_f}{\mu'}\nabla P_f\right) \tag{19}$$

Figure 3 shows the cross-coupling relations between the mechanical field, gas diffusion field, and gas flow field. During the gas extraction process, the fracture pressure in coal affects the change of effective stress and further leads to the change of porosity and permeability. At the same time, the adsorbed gas in the coal matrix diffuses into the fracture system and affects the gas pressure. At this point, 4, 5, 9, 12, 13, 16, and 19 constitute the multifield coupling model.

3. MODEL VALIDATIONS

The user-defined partial differential equation (PDE) module in COMSOL Multiphysics is used to input the governing equations of the physical field, as shown in Figure 3, and the finite element method (FEM) is used to solve these nonlinear PDEs. First, the FEM is used to discretize space to form a series of interrelated small elements, and then a discrete linear algebraic equation set is formed. Finally, the solution on the element node is obtained by solving the equation set. As shown in 20, the most commonly used method to solve this highly nonlinear multiphysical field problem is LU decomposition, that is, the stiffness matrix (K) is decomposed into

https://doi.org/10.1021/acsomega.2c03274
ACS Omega 2022, 7, 29211−29222

the upper triangle matrix (U) and the lower triangle matrix (L), and then the matrix is inversed and solved ($u = U^{-1} L^{-1} F$). The Newton iterative method is an effective method for solving nonlinear problems, that is, using a linear solver to iterate repeatedly to obtain high-precision solutions efficiently. The principle equation is given as follows

$$-\nabla\cdot[c(u)\nabla u] = f \rightarrow Ku = F \quad (20)$$

where c represents the coefficient term of partial differential equations, f represents the source term of the linear system, K represents the matrix of stiffness coefficients, F represents the load vector, and u represents the solution vector.

A single-borehole gas extraction geometric model was created based on the subterranean characteristics of the Guhanshan Mine to test the reasonableness of the multifield coupling model. The buried depth of this coal seam is about 750 m, and gas extraction is carried out by drilling through the layer in the bottom drainage roadway. Figure 4 shows the size

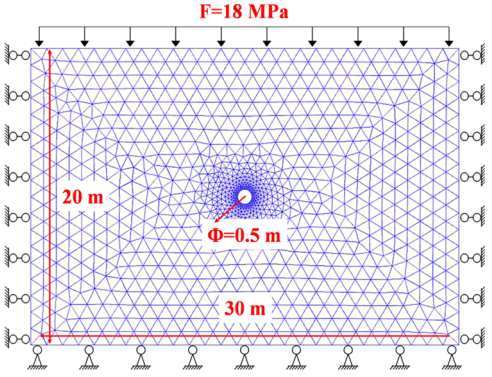

Figure 4. Schematic diagram of the single-borehole gas extraction model.

and boundary conditions of the model. The effective diameter of the hydraulic slotted borehole was set to 0.5 m, and the size of the model was 20 m × 30 m. The upper boundary of the geometric model is a stress load of 18 MPa, the bottom of the model is the fixed constraint boundary, and the left and right sides are set as roller boundaries. The negative pressure of the gas extraction borehole and the initial pressure of the coal seam were set as 16 kPa and 2 MPa, respectively. For the gas flow field, the no-flow boundary is set around the model. The key parameters of the single-borehole gas extraction model are shown in Table 1, and the other parameters are listed in Table 2.

To verify the superiority and accuracy of this model, we compare the simulation results of the new geomechanical-coupled gas flow (GCF) model and the previous model,[36] and take the actual production of gas extraction in the Guhanshan Mine (Henan Province, China) for 60 days as the verification basis.[14] Figure 5 shows the comparative analysis of field test data with numerically simulated data. For the GCF model, it can be seen that there is a small deviation (less than 5%) between the simulation results and the field test results in the first 20 days. Over the next 30 days, the two sets of data are almost identical. After 50 days of gas extraction, the gas pressure around the borehole presents an elliptic distribution, which is related to the anisotropy of coal seam permeability. In general, the curve can fit the test data well. However, for the previous model, the results of the first 30 days are significantly lower than the field test results, and there is also a big gap with the results of the GCF model. Therefore, our GCF model has better accuracy and can guide the layout of extraction boreholes and predict gas production.

Table 1. Guhanshan Coal Parameters

parameter	value	parameter	value
initial porosity of fracture, φ_{f0}	0.0056	initial porosity of the matrix, φ_{p0}	0.06
Langmuir volume constant, a	0.015 m^3/kg	Langmuir pressure constant, b	0.61 MPa^{-1}
density of coal, ρ_c	1250 kg/m^3	Young's modulus of coal, E	2713 MPa
Poisson's ratio, μ	0.34	initial diffusion coefficient, D_0	3×10^{-11} m^2/s
initial permeability in the x-axis direction, k_{x0}	6×10^{-17} m^2	initial permeability in the y-axis direction, k_{y0}	2×10^{-17} m^2

Table 2. Yaxing Coal Parameters

parameter	value	parameter	value
temperature, T	293 K	density of coal, ρ_c	1540 kg/m^3
Langmuir volume constant, a	0.015 m^3/kg	Langmuir pressure constant, b	1 MPa^{-1}
Poisson's ratio, μ	0.42	initial diffusion coefficient, D_0	2×10^{-11} m^2/s
residual diffusion coefficient, D_r	1×10^{-11} m^2/s	attenuation coefficient, ϑ	1×10^{-7} m^2/s
elastic modulus, E	0.92 GPa	volumetric strain threshold, ε_1^V	0.01
elastic modulus of the skeleton, E_p	4.5 GPa	coal strength parameter, F	0.988
initial porosity of fracture, φ_{f0}	0.01	initial porosity of the matrix, φ_{p0}	0.06
initial pressure of coal fracture, P_{f0}	2 MPa	initial pressure of the coal matrix, P_{p0}	2 MPa
initial permeability of coal in the x-axis direction, k_{x0}	3×10^{-16} m^2	initial permeability of coal in the y-axis direction, k_{y0}	1×10^{-16} m^2
elastic modulus of rock, E_r	8 GPa	Poisson's ratio of the rock, μ_r	0.3
initial porosity of the rock, φ_{r0}	0.001	initial permeability of the rock, k_{r0}	3×10^{-21} m^2

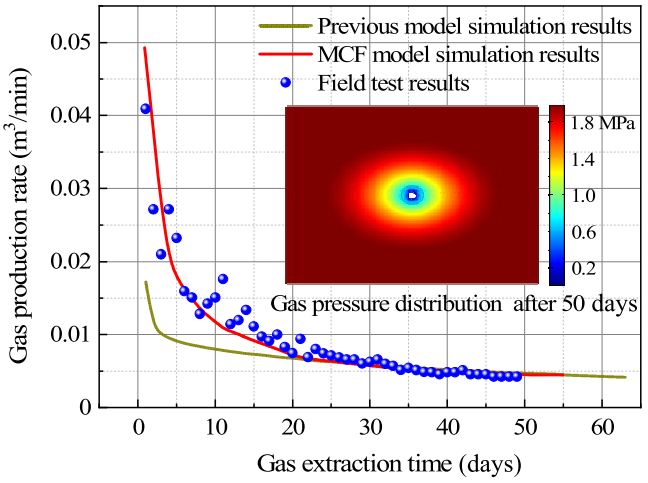

Figure 5. Comparative analysis of field test data with numerical simulated data.

https://doi.org/10.1021/acsomega.2c03274
ACS Omega 2022, 7, 29211−29222

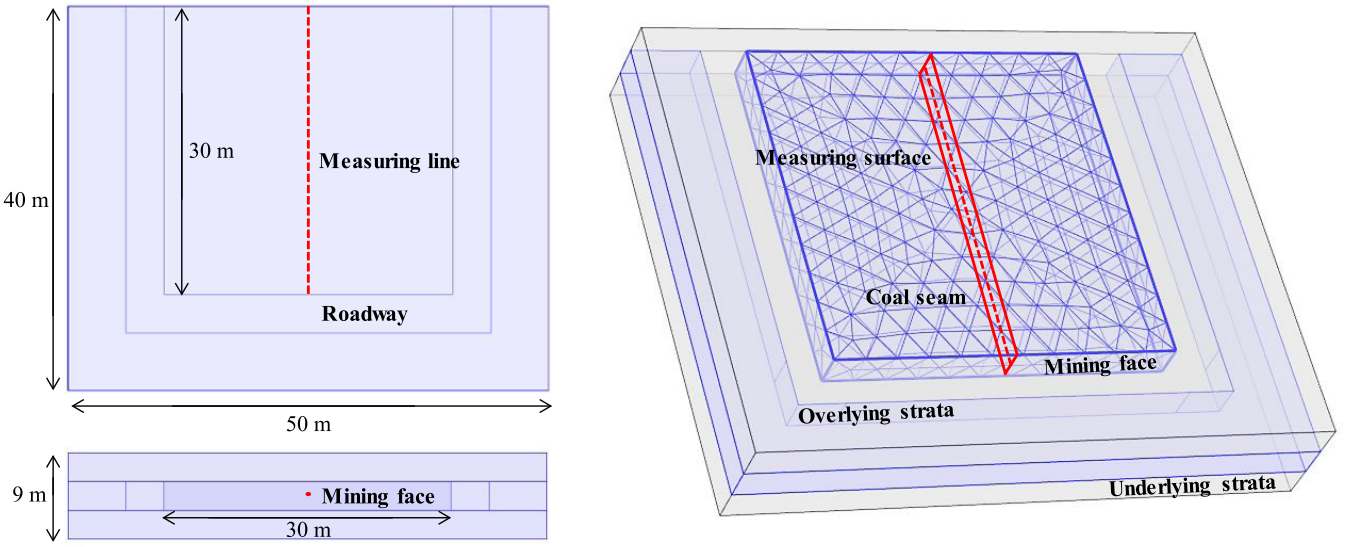

Figure 6. Three-dimensional geometric model.

4. NUMERICAL SIMULATION AND RESULTS

4.1. Division of the Mining-Disturbed Area. During the process of coal mining, the stress state of coal in the mining face changes continuously and has an obvious zoning phenomenon. It can be seen from Figure 1 that this part of coal is divided into three zones: the original stress zone, the stress concentration zone, and the stress-relaxation zone. Therefore, according to the stress−strain state of coal, the stress concentration zone and the stress-relaxation zone are called the mining-disturbed area, and it is considered that plastic deformation mainly occurs in these parts of coal. It is considered that the linear elastic deformation mainly occurs in the original stress zone. To divide the boundary between the two areas, the three-dimensional geometric model, as shown in Figure 6, was established based on the actual situation of the 416 fully mechanized face in the Yaxing Coal Mine. The model is 40 m long, 50 m wide, and 9 m high, and consists of three parts. The middle part is the 4# coal seam (3 m thickness), and the buried depth is about 600 m. The coal seam is surrounded by a roadway with a section size of 4 m × 3 m, and the four walls of the roadway are set as free boundaries. A measuring line and a measuring surface are arranged in the center of the coal seam. Uniaxial loading tests on coal samples show that the elastic modulus of the coal is between 0.47 and 1.39 GPa, with an average of 0.92 GPa, and the Poisson ratio of the coal is between 0.39 and 0.44, with an average of 0.42. Figure 7 shows the fitting relation between the in situ stress and the depth of the coal seam. The data in the figure is from field measurement by Fan et al.,[44] and the fitting result is F_0 = 0.0208H + 2.195. Therefore, the in situ stress of the coal seam buried 600 m deep is 14.6 MPa, and the other parameters of the model are shown in Table 2.

Figure 8 shows the stress distribution of coal in the mining-disturbed area around the underground roadway, and the green dotted line is the boundary between the mining-disturbed area and the original stress area. From Figure 8, with the increase in the distance from the mining face, the first main stress of coal increases rapidly and then decreases slowly, reaching a peak value of about 18.06 MPa at 5 m. As the distance continues to increase, the first main stress begins to decrease and gradually becomes stable after 17 m, and remains

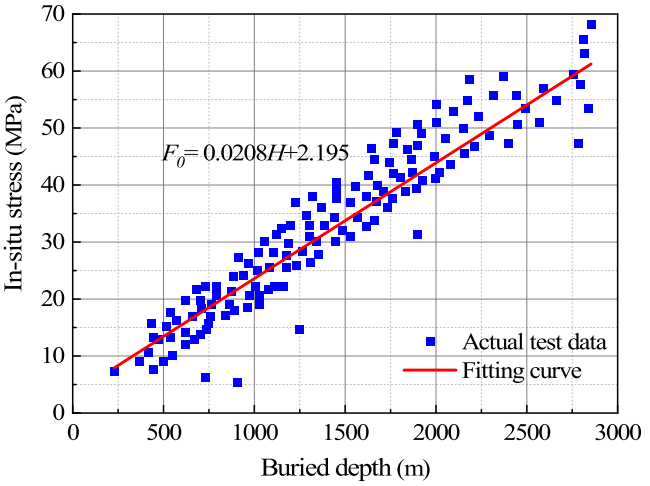

Figure 7. Fitting relation between the in situ stress and the depth of the coal seam.

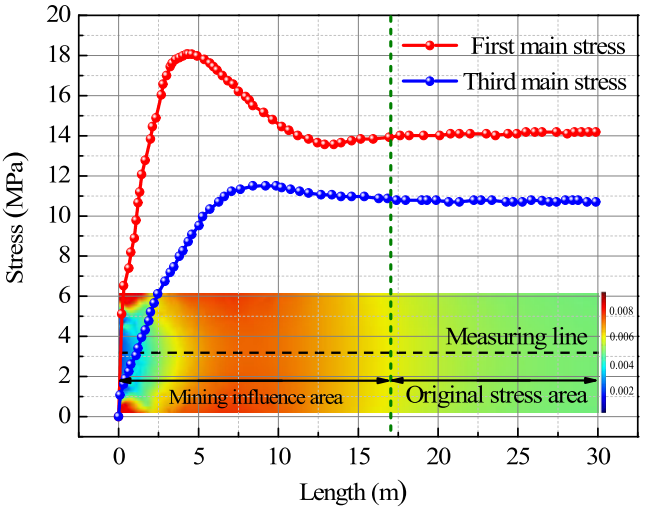

Figure 8. Stress distribution of coal in the mining-disturbed area around the underground roadway.

https://doi.org/10.1021/acsomega.2c03274
ACS Omega 2022, 7, 29211−29222

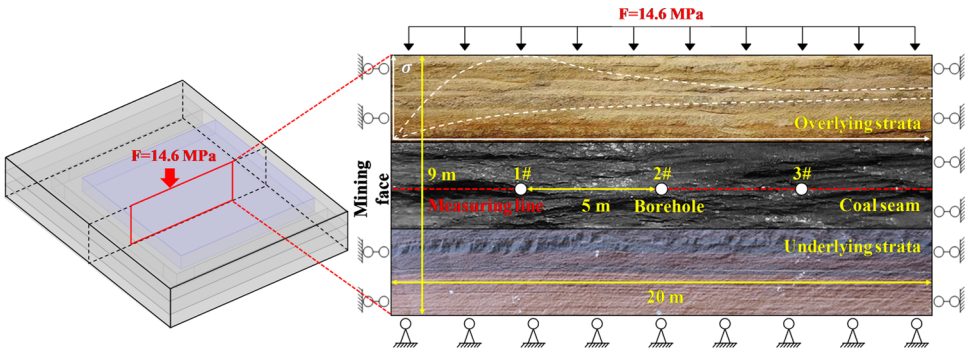

Figure 9. Two-dimensional numerical model.

at about 14.01 MPa. With the increase in the distance from the mining face, the third main stress of the coal increases gradually but the increasing speed decreases gradually. When the distance increases to about 17 m, the third main stress slowly tends to be stable and is maintained at about 10.75 MPa. Therefore, the boundary of the two areas is defined at 17 m, where the front is the mining-disturbed area and the rear is the original stress area. The damage state of coal in these two areas is very different, and the damage factor in the mining-disturbed area is twice as much as the original stress area.

4.2. Numerical Model and Parameters. To further study the physical field evolution law of coal in the mining-disturbed area, a two-dimensional numerical model of gas extraction is established in this paper. As shown in Figure 9, the model is taken from the measuring surface of the 3D model, and its stress state is considered. The model is composed of three parts: The upper part is the overlying strata with a thickness of 3 m, which bears the ground stress of 14.6 MPa (buried depth of 600 m), and the left and right sides are the roller support boundaries. The middle part is the 4# coal seam of 3 m thickness. The left side is the free boundary (mining face) and the right side is the roller support boundary. The lower part is the underlying strata with a thickness of 3 m; the left and right sides are the roller support boundaries and the bottom is the fixed constraint boundary. The size of the model is 20 m × 9 m, and three extraction boreholes with a radius of 0.2 m (spacing 5 m) are set in the coal seam. The initial gas pressure of the coal is 2 MPa, and the pressure of the boreholes is set at 85 kPa. Table 2 shows the basic parameters of the model, mainly from experimental tests and partly from the relevant literature.[36,42] After dividing the model mesh, the finite difference method is used to calculate the node values.

4.3. Dynamic Evolution of the Permeability Field. As can be seen from Figure 10, with the increase in the distance from the mining face, the coal permeability presents a continuous and asymmetric "U"-shaped distribution pattern, that is, the coal permeability first decreases gradually, then increases gradually, and reaches the maximum value near the gas extraction borehole. With the increase in extraction time, the U-shaped low point of permeability gradually increases and the increase rate decreases. The reason is that with the increase in time, the gas pressure of coal fracture decreases slowly, the coal matrix shrinks, the fracture width of coal increases, and the permeability increases gradually. Gas pressure drops quickly in the early stage, so permeability increases greatly and then slows down gradually. After the same time of extraction, the permeability of coal in the range of 0−5 m is significantly higher than that in the range of 5−10 m, while the permeability

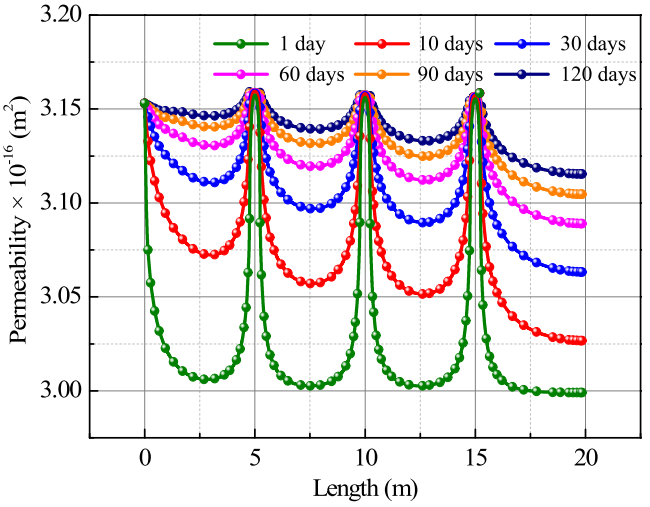

Figure 10. Spatial evolution of permeability.

in the range of 5−10 m is higher than that in the range of 10−15 m. This is because the coal in front of the mining face has different degrees of damage. The stress concentration area is between 0 and 5 m, where the damage degree is the greatest. The further away from this area, the lower the permeability of coal.

Figure 11 shows the contour map of permeability distribution in coal seams after different extraction periods (1, 10, 30, 60, 90, 120 days). After the same time of extraction, the permeability of coal near the mining face is obviously higher but decreases gradually with the increase in the distance. As extraction time increases, the permeability around the boreholes increases slowly. Under the influence of anisotropy, the permeability contour shows an elliptic distribution law. After 60 days of gas extraction, a fan-shaped distribution of permeability can be obviously observed. This is because after the gas pressure inside the coal decreases, the effective stress gradually increases, resulting in the damage effect gradually becoming prominent. Taking 120 days of gas extraction as an example, it can be found that permeability around the boreholes has the following rule: 1#> 2#> 3#. This is because the 1# borehole is located in the stress concentration area of the mining-disturbed coal seam (as shown in Figure 9), and the coal has a larger damage factor, so its permeability is higher. However, as the distance from the mining face increases, the coal stress gradually transitions to the state of hydrostatic pressure, and then the coal damage factor and permeability are both small.

https://doi.org/10.1021/acsomega.2c03274
ACS Omega 2022, 7, 29211−29222

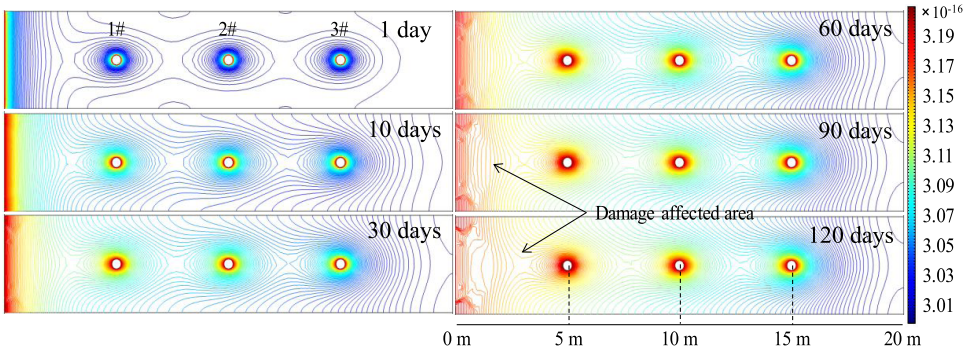

Figure 11. Temporal evolution of coal seam permeability.

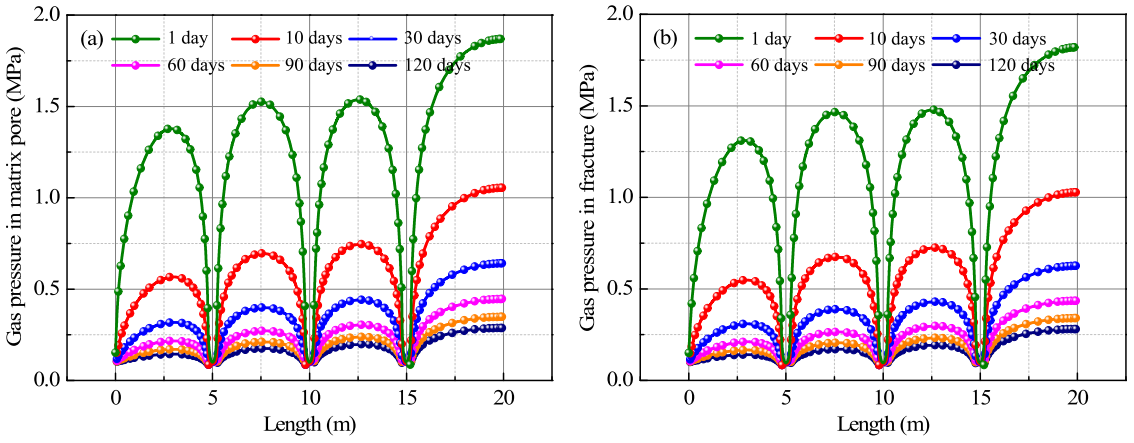

Figure 12. Spatial evolutions of coal seam gas pressure. (a) Matrix and (b) fracture.

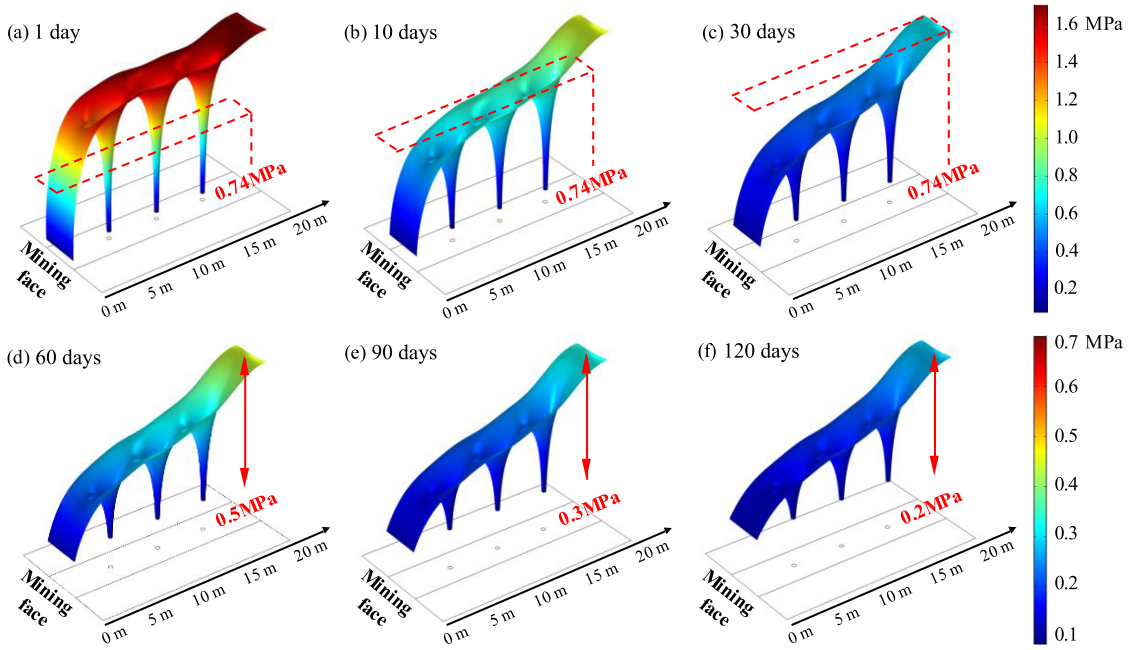

Figure 13. Temporal evolution of gas pressure in the matrix. (a) 1 day, (b) 10 days, (c) 30 days, (d) 60 days, (e) 90 days, and (f) 120 days.

4.4. Dynamic Evolution of the Gas Flow Field. Figure 12 shows the variation of the coal matrix and fracture gas pressure at different distances from the mining face. From Figure 12, the gas pressure distribution starts presenting a continuous "n"-shaped distribution pattern with different sizes. As the distance from the mining face increases, the n-shaped peak value gradually increases, which is related to the variation law of porosity. As the extraction time increases, the gas pressure in the matrix and fracture both decreased gradually. By comparing Figure 12a,b, it can be found that the gas pressure in the coal matrix is slightly larger than that in the fracture, and the former is about 3% larger than the latter. This

https://doi.org/10.1021/acsomega.2c03274
ACS Omega 2022, 7, 29211−29222

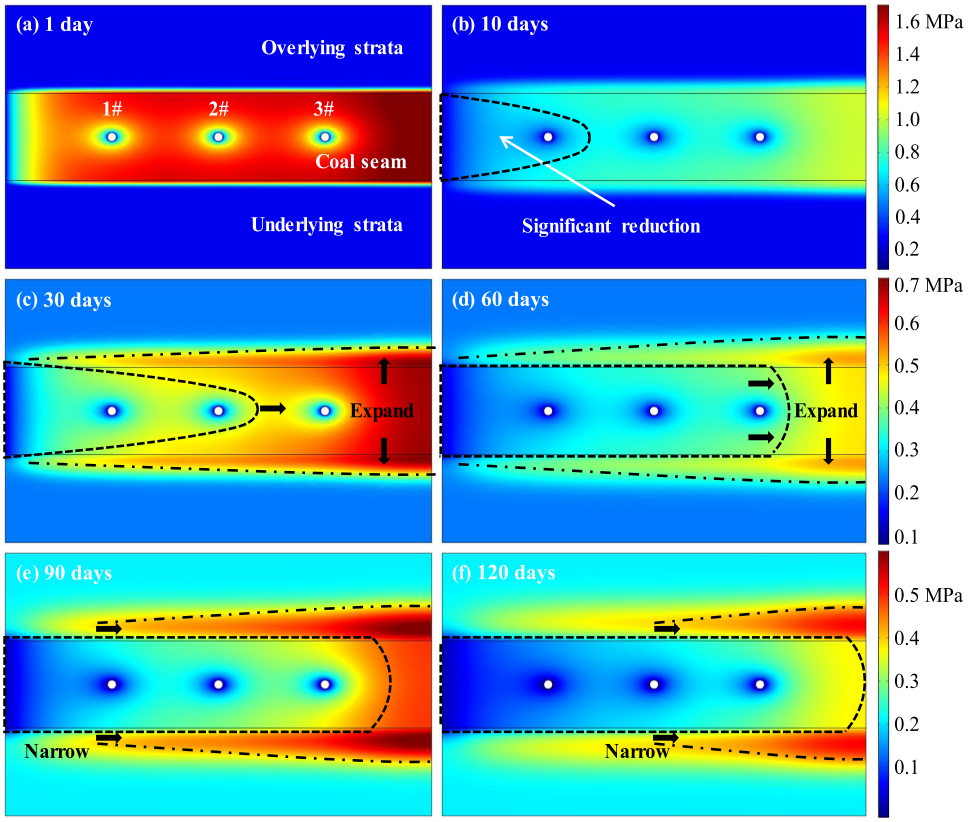

Figure 14. Temporal evolution of gas pressure in fracture. (a) 1 day, (b) 10 days, (c) 30 days, (d) 60 days, (e) 90 days, and (f) 120 days.

is because the adsorbed gas in the coal is continuously desorbed and first diffuses into the pores of the coal matrix and then slowly enters into the fracture of the coal, with a certain lag. After the same time of gas extraction, the gas pressure drop of coal around the 1# borehole is the largest, which is obviously higher than that of the 2# borehole and the 3# borehole. This is because the damage and porosity of coal around the 1# borehole are large, so its gas extraction effect is the best.

Figure 13 shows the gas pressure distribution of the coal matrix after different extraction periods (1, 10, 30, 60, 90, 120 days). As shown in Figure 13, it is obvious that the gas pressure on the mining face and the coal matrix near the gas extraction boreholes is very low. With the increase in the length, the content of gas in the matrix gradually increases, reaching the maximum value at 20 m. According to the literature,[45] the safe area of gas extraction is defined as the area where gas pressure drops below 0.74 MPa. From Figure 13a, it can be seen that the safe area of gas extraction is very small and the effect of gas extraction is poor. As shown in Figure 13b, after 10 days of gas extraction, the safe area of gas extraction is increased to about 10 m from the mining face. Figure 13c shows that the gas pressure of the coal matrix in the mining-disturbed area is lower than 0.74 MPa, which indicates that the gas pressure of the coal seam drops significantly after 30 days of gas extraction, and the coal mining process is safe. As shown in Figure 13d−f, as the extraction time increases, the gas pressure of the coal seam decreases, and the decline is gradual.

Figure 14 shows the gas pressure distribution in fracture after different gas extraction periods (1, 10, 30, 60, 90, 120 days). From Figure 14b, it can be seen that the gas pressure of the coal fracture within the range of 0−5 m significantly reduces, and the safe area of gas extraction in the mining face presents a triangular distribution. With the increase in gas extraction time, this area has a trend of horizontal expansion. As shown in Figure 14c,d, the gas pressure in fracture between the coal seam and upper and lower strata tends to increase, and the phenomenon of "gas flow in strata" appears. This is because driven by the pressure difference, the fracture gas of the coal seam gradually flows to the fracture of the upper and lower overburden strata, and the influence range gradually increases. According to Figure 14e,f, starting from the mining face, the gas flow range in the upper and lower strata gradually narrows. This is because the permeability of coal around the 1# borehole is relatively high, and the gas in the coal fracture drops rapidly.

5. DISCUSSION

In the second and third sections, we introduced the geomechanical-coupled gas flow (GCF) model and analyzed the flow field evolution. Compared with previous models,[36] this model has the following improvements: (a) Considering the damage and degradation effect of the elastic modulus after the coal is damaged by geological stress, the GCF model can better reveal the multifield coupling law of the coal seam during coal mining. (b) Based on experimental verification, the diffusion coefficient in this work decreases dynamically with time. Compared with the fixed diffusion coefficient of the traditional single pore model, the current governing equation of matrix gas diffusion can better describe the multistage pore coal model. The research results can improve the understanding of the stress field, permeability field, and gas flow field evolution law of the mining-disturbed coal seam. However, it is

https://doi.org/10.1021/acsomega.2c03274
ACS Omega 2022, 7, 29211−29222

still necessary to discuss the effectiveness of gas extraction and environmental benefits through a case study.

The variation of coal seam gas content is the key factor to judge the effect of gas extraction. Figure 15 shows the dynamic

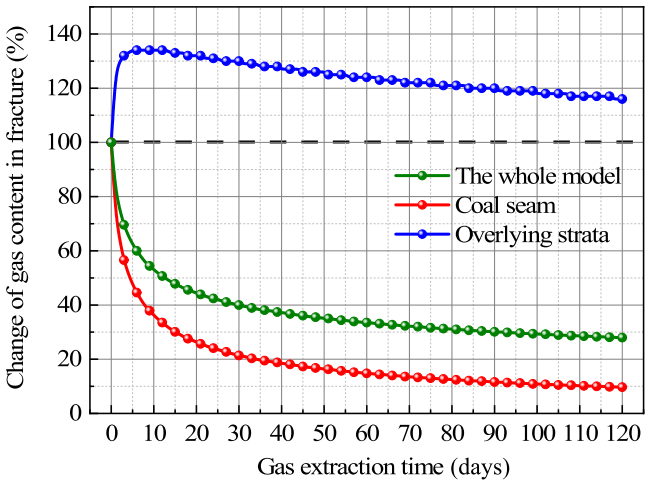

Figure 15. Dynamic evolution of gas content with extraction time.

evolution of gas content with extraction time. Based on the analysis of 416 fully mechanized face of the Yaxing Coal Mine, with the increase in gas extraction time, the gas content in the coal seam and the whole model shows a trend of rapid decline and then a slow decline, with a decrease of 90 and 82%, respectively. However, the gas content in the overlying strata shows a trend of a rapid rise and then a slow decline, reaching a peak of 134% at 10 days. Combined with the previous section, it can be found that when gas extraction exceeds 30 days, the 4# coal seam can achieve a better gas control effect, and the gas content of the coal seam is only 20% at this time. However, the gas content in the overlying strata began to decline, and the leakage of coal-mine gas from it was not effectively reduced. Therefore, only gas drainage along the coal seam can not effectively control the greenhouse gas leakage.

During the mining process, abnormal coal-mine gas emissions and gas over the safety limit in goaf often occur, which have seriously affected the safety of daily coal mining. As shown in Figure 16, the reasons leading to the above problems are various. According to the analysis results of the permeability model established above, it can be found that there are two main reasons. On the one hand, with the increase in the mining depth of this mine, there is no effective gas extraction during coal seam mining. Moreover, the coal in the mining face is affected by the mining disturbance, which causes the gas in the coal fracture to flow rapidly to the 416 goaf. On the other hand, the 415 goaf is directly above the 416 fully mechanized face of this mine. They are both in the 4# coal seam, and the distance between the two areas is 10−25 m. The roof of the 416 mining face is mainly composed of siltstone and sandy mudstone, and the permeability coefficient is larger, which is thousands of times higher than that of shale. According to Figure 14 of the simulation results, the phenomenon of gas flow in strata can occur in the sandstone roof with high permeability. Moreover, there is a large amount of residual coal in the 415 goaf, and the free gas in the residual coal may flow to the 416 goaf through the fracture of the overlying strata. When there is no gas extraction project in the coal seam, a large amount of methane gas escapes into the goaf from the overlying strata and mining face, causing pollution and danger. Therefore, it is not only necessary to carry out gas extraction in this coal seam but also to carry out interlayer gas extraction in the overlying strata. In the design of 4# coal seam gas extraction, the interval of boreholes is set at 5 m according to the dynamic evolution law of gas flow. At the same time, extraction boreholes are set vertically upward, and extraction pipes over 8 m are arranged. Through the on-site extraction engineering practice, coalbed methane emissions are reduced by more than half, which not only reduces GHG pollution but also solves the problem of coal-mine gas safety.

6. CONCLUSIONS

In this study, a geomechanical-coupled gas flow model is used to detect greenhouse gas pollution. This model takes gas extraction at the 416 fully mechanized face of the Yaxing Coal Mine as engineering background, and the main conclusions are as follows:

(1) By introducing the dynamic diffusion coefficient and considering the coal damage, the gas production rate of anisotropic coal with single-borehole gas extraction is simulated and analyzed. Moreover, the simulated data are matched with the field test data of the Guhanshan Coal Mine, and the gas production of the two is consistent, which verifies the rationality and accuracy of the model.

(2) The first main stress of coal in the mining-disturbed area increases gradually and then decreases slowly, and reaches the peak value at 5 m. The third principal stress increases gradually at first and becomes stable after 10 m. The coal permeability and gas pressure show continuous and asymmetric U-shaped and n-shaped

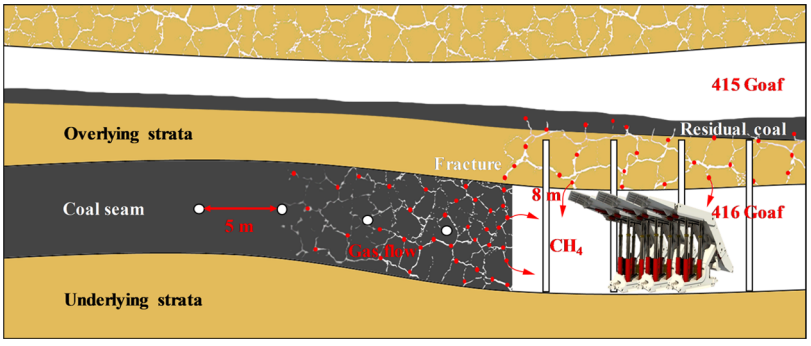

Figure 16. Illustration of gas flow in the goaf residual coal and the mining-disturbed coal seam.

https://doi.org/10.1021/acsomega.2c03274
ACS Omega 2022, 7, 29211−29222

distribution characteristics, respectively. Under the influence of coal damage caused by in situ stress, the gas extraction effect of the 1# borehole is better than that of 2# and 3# boreholes.

(3) The gas content of the coal seam first drops rapidly and then drops slowly, and the safe area of gas extraction presents a triangle distribution and shows a trend of lateral expansion. However, the gas content of the overlying strata shows a trend of a rapid rise first and then a slow decline. The research results guide the solution to the abnormal gas emission disaster of the 4# coal seam and provide theoretical support for reducing greenhouse gas emissions.

AUTHOR INFORMATION

Corresponding Author

Zheng Zhong − *School of Science, Harbin Institute of Technology, Shenzhen 518055, P. R. China*; orcid.org/0000-0001-6037-8185; Email: zhongzheng@hit.edu.cn

Authors

Haoran Song − *School of Science, Harbin Institute of Technology, Shenzhen 518055, P. R. China*

Baiquan Lin − *School of Safety Engineering, China University of Mining and Technology, Xuzhou 221116, P. R. China*

Ting Liu − *School of Safety Engineering, China University of Mining and Technology, Xuzhou 221116, P. R. China*

Complete contact information is available at: https://pubs.acs.org/10.1021/acsomega.2c03274

Notes

The authors declare no competing financial interest.

ACKNOWLEDGMENTS

This work was supported by the National Natural Science Foundation of China (Grant No. 11932005).

REFERENCES

(1) Karacan, C.Ö.; Ruiz, F. A.; Cote, M.; Phipps, S. Coal mine methane: A review of capture and utilization practices with benefits to mining safety and to greenhouse gas reduction. *Int. J. Coal Geol.* **2011**, *86*, 121−156.

(2) Ranathunga, A. S.; Perera, M. S. A.; Ranjith, P. G. Deep coal seams as a greener energy source: a review. *J. Geophys. Eng.* **2014**, *11*, No. 063001.

(3) Zou, Q.; Zhang, T.; Ma, T.; Tian, S.; Jia, X.; Jiang, Z. Effect of water-based SiO2 nanofluid on surface wettability of raw coal. *Energy* **2022**, *254*, No. 124228.

(4) Liu, T.; Lin, B. Q.; Fu, X. H.; Zhu, C. J. Modeling air leakage around gas extraction boreholes in mining-disturbed coal seams. *Process Saf. Environ.* **2020**, *141*, 202−214.

(5) Qianting, H.; Liang, Y. P.; Wang, H.; Zou, Q. L.; Sun, H. T. Intelligent and integrated techniques for coalbed methane (CBM) recovery and reduction of greenhouse gas emission. *Environ. Sci. Pollut. Res.* **2017**, *24*, 17651−17668.

(6) Li, Y. K.; Wu, S. Y.; Nie, B. S.; Ma, Y. K. A new pattern of underground space-time tridimensional gas drainage: A case study in Yuwu coal mine, China. *Energy Sci. Eng.* **2019**, *7*, 399−410.

(7) Szkudlarek, Z.; Janas, S. Active protection of work area against explosion of dust−gas mixture. *Int. J. Coal Sci. Technol.* **2021**, *8*, 11.

(8) Song, H. R.; Zhong, Z. Mechanical Degradation Model of Porous Coal Invaded by Water Molecules. *SSRN Electron. J.* **2022**, DOI: 10.2139/ssrn.4081795.

(9) Chen, B. Stress-induced trend:the clustering feature of coal mine disasters and earthquakes in China. *Int J. Coal Sci. Technol.* **2020**, *7*, 676−692.

(10) Fan, Z. L.; Fan, G. W.; Zhang, D. S.; Zhang, L.; Zhang, S.; Liang, S. S.; Yu, W. Optimal injection timing and gas mixture proportion for enhancing coalbed methane recovery. *Energy* **2021**, *222*, No. 119880.

(11) Zou, Q. L.; Zhang, T. C.; Cheng, Z. H.; Jiang, Z. B.; Tian, S. X. A method for selection rationality evaluation of the first-mining seam in multi-seam mining. *Geomech. Geophys. Geo-Energy Geo-Resour.* **2022**, *8*, No. 72.

(12) Wu, C.; Yuan, C.; Wen, G.; Han, L.; Liu, H. A dynamic evaluation technique for assessing gas output from coal seams during commingling production within a coalbed methane well: a case study from the Qinshui Basin. *Int. J. Coal Sci. Technol.* **2020**, *7*, 11.

(13) An, F. H.; Wang, Z. F.; Yang, H. M.; Yang, S. Y.; Pan, F. M.; Chen, T.; Xie, C. Application of directional boreholes for gas drainage of adjacent seams. *Int. J. Rock Mech. Min.* **2016**, *90*, 35−42.

(14) Zhao, Y.; Lin, B. Q.; Liu, T.; Kong, J.; Zheng, Y. N. Gas flow in hydraulic slotting-disturbed coal seam considering stress relief induced damage. *J. Nat. Gas Sci. Eng.* **2020**, *75*, No. 103160.

(15) Si, G. Y.; Belle, B. Performance analysis of vertical goaf gas drainage holes using gas indicators in Australian coal mines. *Int. J. Coal Geol.* **2019**, *216*, No. 103301.

(16) Chen, X. Z.; Xue, S.; Yuan, L. Coal seam drainage enhancement using borehole presplitting basting technology - A case study in Huainan. *Int. J. Min. Sci. Technol.* **2017**, *27*, 771−775.

(17) Goraya, N. S.; Rajpoot, N.; Sivagnanam, B. M. Coal Bed Methane Enhancement Techniques: A Review. *ChemistrySelect* **2019**, *4*, 3585−3601.

(18) Si, G. Y.; Durucan, S.; Shi, J. Q.; Korre, A.; Cao, W. Z. Parametric Analysis of Slotting Operation Induced Failure Zones to Stimulate Low Permeability Coal Seams. *Rock Mech. Rock Eng.* **2019**, *52*, 163−182.

(19) Lin, M. H.; Lin, B. Q.; Yang, W.; Zhao, Y.; Wang, Z. In-situ testing method of the permeability coefficient in a coal seam based on the finite volume method and its application. *J. Nat. Gas Sci. Eng.* **2022**, *97*, No. 104370.

(20) Guo, C.; Lin, B. Q.; Yao, H.; Yang, K.; Zhu, C. J. Characteristics of breaking coal-rock by submerged jet and its application on enhanced coal bed methane recovery. *Energy Source, Part A* **2020**, *42*, 2249−2260.

(21) Zhang, H. B.; Liu, J. S.; Elsworth, D. How sorption-induced matrix deformation affects gas flow in coal seams: A new FE model. *Int. J. Rock Mech. Min.* **2008**, *45*, 1226−1236.

(22) Lu, S. Q.; Cheng, Y. P.; Li, W. Model development and analysis of the evolution of coal permeability under different boundary conditions. *J. Nat. Gas Sci. Eng.* **2016**, *31*, 129−138.

(23) Wang, G. D.; Ren, T.; Wang, K.; Zhou, A. T. Improved apparent permeability models of gas flow in coal with Klinkenberg effect. *Fuel* **2014**, *128*, 53−61.

(24) Peng, Y.; Liu, J. S.; Pan, Z. J.; Connell, L. D.; Chen, Z. W.; Qu, H. Y. Impact of coal matrix strains on the evolution of permeability. *Fuel* **2017**, *189*, 270−283.

(25) Zhang, Z. T.; Zhang, U.; Xie, H. P.; Gao, M. Z.; Zha, E. S.; Jia, Z. Q. An anisotropic coal permeability model that considers mining induced stress evolution, microfracture propagation and gas sorption desorption effects. *J. Nat. Gas Sci. Eng.* **2017**, *46*, 664−679.

(26) Dejam, M. Hydrodynamic dispersion due to a variety of flow velocity profiles in a porous-walled microfluidic channel. *Int. J. Heat Mass Transfer* **2019**, *136*, 87−98.

(27) Fang, H. H.; Sang, S. X.; Liu, S. Q. Establishment of dynamic permeability model of coal reservoir and its numerical simulation during the CO2-ECBM process. *J. Pet. Sci. Eng.* **2019**, *179*, 885−898.

(28) Xie, H. P.; Zhou, H. W.; Liu, J. F.; Gao, F.; Zhang, Y. Mining-induced mechanical behavior in coal seams under different mining layouts. *J. China Coal Soc.* **2011**, *36*, 1067−1074.

(29) Xue, Y.; Gao, F.; Liu, X. G. Effect of damage evolution of coal on permeability variation and analysis of gas outburst hazard with coal mining. *Nat. Hazards* **2015**, *79*, 999−1013.
(30) Lu, S. Q.; Zhang, Y. L.; Sa, Z. Y.; Si, S. F.; Shu, L. Y.; Wang, L. Damage-induced permeability model of coal and its application to gas predrainage in combination of soft coal and hard coal. *Energy Sci Eng.* **2019**, *7*, 1352−1367.
(31) Zheng, C. S.; Kizil, M. S.; Chen, Z. W.; Aminossadati, S. M. Role of multi-seam interaction on gas drainage engineering design for mining safety and environmental benefits: Linking coal damage to permeability variation. *Process Saf. Environ. Prot.* **2018**, *114*, 310−322.
(32) An, F. H.; Cheng, Y. P.; Wang, L.; Li, W. A numerical model for outburst including the effect of adsorbed gas on coal deformation and mechanical properties. *Comput. Geotech.* **2013**, *54*, 222−231.
(33) Liu, T.; Lin, B. Q.; Fu, X. H.; Liu, S. M. A new approach modeling permeability of mining-disturbed coal based on a conceptual model of equivalent fractured coal. *J. Nat. Gas Sci. Eng.* **2020**, *79*, No. 103366.
(34) Chen, Y. X.; Chu, T. X.; Chen, X. X.; Chen, P. Coupling of stress and gas pressure in dual porosity medium during coal seam mining. *Powder Technol.* **2020**, *367*, 390−398.
(35) Zhao, Y.; Lin, B. Q.; Liu, T.; Li, Q. Z.; Kong, J. Gas flow field evolution around hydraulic slotted borehole in anisotropic coal. *J. Nat. Gas Sci. Eng.* **2018**, *58*, 189−200.
(36) Lin, B. Q.; Song, H. R.; Zhao, Y.; Liu, T.; Kong, J.; Huang, Z. B. Significance of gas flow in anisotropic coal seams to underground gas drainage. *J. Pet. Sci. Eng.* **2019**, *180*, 808−819.
(37) Liu, T.; Lin, B. Q.; Yang, W.; Liu, T.; Kong, J.; Huang, Z. B.; Wang, R.; Zhao, Y. Dynamic diffusion-based multifield coupling model for gas drainage. *J. Nat. Gas Sci. Eng.* **2017**, *44*, 233−249.
(38) Hu, S. B.; Wang, E. Y.; Liu, X. F. Effective stress of gas-bearing coal and its dual pore damage constitutive model. *Int. J. Damage Mech.* **2016**, *25*, 468−490.
(39) Salari, M. R.; Saeb, S.; Willam, K. J.; Patchet, S. J.; Carrasco, R. C. A coupled elastoplastic damage model for geomaterials. *Comput. Method Appl. Mech. Eng.* **2004**, *193*, 2625−2643.
(40) Zhu, Q. Z.; Shao, J. F.; Mainguy, M. A micromechanics-based elastoplastic damage model for granular materials at low confining pressure. *Int. J. Plast.* **2010**, *26*, 586−602.
(41) Palmer, I. Permeability changes in coal: Analytical modeling. *Int. J. Coal Geol.* **2009**, *77*, 119−126.
(42) Zhao, Y.; Lin, B. Q.; Liu, T.; Zheng, Y. N.; Kong, J.; Li, Q. Z.; Song, H. R. Mechanism of multifield coupling-induced outburst in mining-disturbed coal seam. *Fuel* **2020**, *272*, No. 117716.
(43) Liu, T.; Lin, B. Q.; Fu, X. H.; Gao, Y. B.; Kong, J.; Zhao, Y.; Song, H. R. Experimental study on gas diffusion dynamics in fractured coal: A better understanding of gas migration in in-situ coal seam. *Energy* **2020**, *195*, No. 117005.
(44) Fan, C. J.; Sheng, L. I.; Luo, M. K.; Yang, Z. H.; Zhang, H. H.; Wang, S. Deep CBM extraction numerical simulation based on hydraulic-mechanicalthermal coupled model. *J. China Coal Soc.* **2016**, *41*, 3076−3085.
(45) Zhang, C. L.; Xu, J.; Peng, S. J.; Li, Q. X.; Yan, F. Z. Experimental study of drainage radius considering borehole interaction based on 3D monitoring of gas pressure in coal. *Fuel* **2019**, *239*, 955−963.

https://doi.org/10.1021/acsomega.2c03274
ACS Omega 2022, 7, 29211−29222